Nonlinear, Band-structure, and Surface Effects in the Interaction of Charged Particles with Solids

J. M. Pitarke[1,2], I. G. Gurtubay[1], and V. U. Nazarov[3]
[1]Materia Kondentsatuaren Fisika Saila, UPV/EHU,
644 Posta Kutxatila, E-48080 Bilbo, Basque Country
[2]Donostia International Physics Center (DIPC) and
Centro Mixto CSIC-UPV/EHU, Basque Country
[3]Department of Physics and Institute for Condensed
Matter Theory, Chonnam National University,
Kwangju 500-757, Korea

February 2, 2008

Abstract

A survey is presented of various aspects of the interaction of charged particles with solids. In the framework of many-body perturbation theory, we study the nonlinear interaction of charged particles with a free gas of interacting electrons; in particular, nonlinear corrections to the stopping power are analyzed, and special emphasis is made on the separate contributions that are originated in the excitation of either electron-hole pairs, single plasmons, or double plasmons. Ab initio calculations of the electronic energy loss of ions moving in real solids are also presented, and the energy loss of charged particles interacting with simple metal surfaces is addressed.

Contents

1 Introduction **3**

2 Theory **5**
2.1 Uniform electron gas 8
2.1.1 High-velocity limit 9
2.1.2 Double-plasmon excitation 10
2.2 Bounded electron gas 12
2.2.1 Parallel trajectory 13
2.2.2 High-velocity limit 13
2.3 Periodic crystals 14

3 Results **16**
3.1 Uniform electron gas 16
3.1.1 Stopping power 16
3.1.2 Double-plasmon excitation 23
3.2 Bounded electron gas 24
3.3 Periodic crystals 27
3.3.1 Random stopping power 28

4 Summary and conclusions **29**

1 Introduction

A quantitative description of the interaction of charged particles with solids is of basic importance in many different theoretical and applied areas [1]. When a moving charged particle penetrates a solid material, it may lose energy to the medium through various elastic and inelastic collision processes that are based on electron excitation and nuclear recoil motion in the solid. While energy losses due to nuclear recoil may become dominant at very low energies of the projectile [2], in the case of electrons or ions moving with nonrelativistic velocities that are comparable to the mean speed of electrons in the solid the most significant energy losses are due to the generation of electronic excitations, such as electron-hole (e-h) pairs, collective excitations, i.e., plasmons, and inner-shell excitations and ionizations.

In 1913 Niels Bohr published a seminal paper on the energy loss of charged particles interacting with electrons bound to atoms [3], which laid the ground for Bethe's quantum theory of stopping power [4]. The many-body problem of interacting conduction electrons in metals was investigated by Bohm and Pines [5] in the so-called *jellium* model, by simply replacing the ionic lattice of the solid by a homogeneous background which serves to provide neutrality to the system. Within linear-response theory, the electronic response of conduction electrons to external charged particles is determined by a wavevector- and frequency-dependent longitudinal dielectric function. In the self-consistent-field, or random-phase, approximation (RPA), the dielectric function of interacting free electrons was derived by Lindhard [6], and, subsequently, a number of workers have derived alternative dielectric functions that incorporate various many-body higher-order local-field corrections [7, 8] and band-structure effects [9]. The effect of dissipative processes occurring in a real metal and conversion of plasmons into multiple e-h pairs has been allowed phenomenologically by including a damping coefficient in the dielectric function [10].

The validity of linear-response theory, which treats the perturbing potential to lowest order, is not obvious a priori. While lowest-order perturbation theory leads to energy losses that are proportional to the square of the projectile charge $Z_1 e$, the energy loss of either positive and negative pions [11] or protons and antiprotons [12, 13] is known to exhibit a measurable dependence on the sign of the charge [14, 15, 16]. Experimentally observed nonlinear double-plasmon excitations [17, 18] are also beyond the realm of standard linear-response theory [19, 20, 21], nonlinearities may play an im-

portant role in the electronic wake generated by moving ions in solids [22, 23], and lowest-order perturbation theory breaks down when the projectile is capable of carrying bound electrons with it [24].

The first full nonlinear calculation of the electronic stopping power of an electron gas was performed by Echenique *et al.* [25], in the low-velocity limit. They used a scattering approach to the stopping power, and the scattering cross sections were calculated for a statically screened potential which was determined self-consistently by using density-functional theory (DFT) [26]. These static-screening calculations were then extended to projectile velocities approaching the Fermi velocity of the target [27]. Alternatively, an effective charge can be assigned to the projectile [28] and nonlinearities can then be investigated within quadratic-response theory, thereby providing results for arbitrary projectile velocities [29].

To calculate the electronic stopping power of real solids from the knowledge of the full band structure of the solid and the corresponding Bloch eigenfunctions and eigenvalues is a laborious problem. Hence, early theoretical investigations were based on semiempirical treatments of the electronic excitations in the solid [30, 31, 32, 33, 34]. Attemps to introduce the full electronic band structure in the evaluation of the electronic stopping power of alkaline metals for low projectile velocities include a one-band calculation [35] as well as a calculation based on a linear combination of atomic orbitals [36]. The low-velocity limit was also investigated, in the case of silicon, on the basis of a static treatment of the density response of the solid [37]. Ab initio band-structure calculations that are based on a full evaluation of the dynamical density-response of the solid have been carried out only very recently [38, 39, 40].

In this paper, we summarize recent investigations on the impact of nonlinear, band-structure, and surface effects in the interaction of charged particles with solids. We present general procedures to calculate, within many-body perturbation theory, the nonlinear potential induced by moving ions in an interacting free-electron gas (FEG), Z_1^3 contributions to the stopping power of a FEG, and double-plasmon excitation probabilities. Self-consistent calculations of the energy-loss spectra of charged particles moving near a metal surface are also presented. Finally, we consider the electronic stopping power of valence electrons in real solids, which we evaluate within random conditions.

Unless otherwise is stated, atomic units are used throughout this paper, i.e., $e^2 = \hbar = m_e = 1$. The atomic unit of length is the Bohr radius,

$a_0 = \hbar^2/m_e^2 = 0.529\,\text{Å}$, the atomic unit of energy is the Hartree, $1\,\text{Hartree} = e^2/a_0 = 27.2\,\text{eV}$, and the atomic unit of velocity is the Bohr velocity, $v_0 = \alpha\, c = 2.19 \times 10^8\,\text{cm}\,\text{s}^{-1}$, α and c being the fine structure constant and the velocity of light, respectively.

2 Theory

We consider a recoiless particle of charge Z_1 [41] moving in an arbitrary inhomogeneous electron system with nonrelativistic velocity $\mathbf{v}$, for which retardation effects and radiation losses can be neglected. The energy that the probe particle loses per unit time due to electronic excitations in the medium can be written as [42]

$$-\frac{dE}{dt} = -\int d\mathbf{r}\, \rho^{ext}(\mathbf{r},t)\, \frac{\partial V^{ind}(\mathbf{r},t)}{\partial t}, \tag{1}$$

where $\rho^{ext}(\mathbf{r},t)$ represents the probe-particle charge density

$$\rho^{ext}(\mathbf{r},t) = Z_1\, \delta(\mathbf{r} - \mathbf{r}_0 - \mathbf{v}\, t) \tag{2}$$

and $V^{ind}(\mathbf{r},t)$ is the induced potential. Keeping terms of first and second order in the external perturbation, time-dependent perturbation theory yields

$$\begin{aligned} V^{ind}(\mathbf{r},t) &= \int d\mathbf{r}' \int_{-\infty}^{+\infty} dt' \int_{-\infty}^{+\infty} \frac{d\omega}{2\pi}\, \mathrm{e}^{-i\omega(t-t')} \int d\mathbf{r}_1 \int d\mathbf{r}_3\, v(\mathbf{r},\mathbf{r}_1) \\ &\times \left[\chi(\mathbf{r}_1,\mathbf{r}_3;\omega) + \int d\mathbf{r}'' \int_{-\infty}^{+\infty} dt'' \int_{-\infty}^{+\infty} \frac{d\omega'}{2\pi} \mathrm{e}^{-i(\omega+\omega')(t'-t'')} \right. \\ &\times \left. \int d\mathbf{r}_2\, Y(\mathbf{r}_1,\mathbf{r}_2,\mathbf{r}_3;\omega,\omega')\, v(\mathbf{r}_2,\mathbf{r}'')\, \rho^{ext}(\mathbf{r}'',t'') \right] v(\mathbf{r}_3,\mathbf{r}')\, \rho^{ext}(\mathbf{r}',t'), \end{aligned} \tag{3}$$

where $v(\mathbf{r},\mathbf{r}') = 1/|\mathbf{r}-\mathbf{r}'|$ is the bare Coulomb interaction, and $\chi(\mathbf{r}_1,\mathbf{r}_2;\omega)$ and $Y(\mathbf{r}_1,\mathbf{r}_2,\mathbf{r}_3;\omega,\omega')$ are the so-called linear and quadratic density-response functions of the electron system:

$$\chi(\mathbf{r}_1,\mathbf{r}_2;\omega) = \frac{1}{\Omega} \sum_n \left[\frac{[\hat{\rho}(\mathbf{r}_1)]_{0n}\, [\hat{\rho}(\mathbf{r}_2)]_{n0}}{\omega - \omega_{n0} + \mathrm{i}\eta} - \frac{[\hat{\rho}(\mathbf{r}_2)]_{0n}\, [\hat{\rho}(\mathbf{r}_1)]_{n0}}{\omega + \omega_{n0} + \mathrm{i}\eta} \right] \tag{4}$$

and

$$Y(\mathbf{r}_1,\mathbf{r}_2,\mathbf{r}_3;\omega,\omega') = -\frac{1}{2\Omega} \sum_{n,l} \left[\frac{[\hat{\rho}(\mathbf{r}_1)]_{0n}\, [\hat{\rho}(\mathbf{r}_3)]_{nl}\, [\hat{\rho}(\mathbf{r}_2)]_{l0}}{[\omega - \omega_{n0} + \mathrm{i}\eta]\, [\omega' + \omega_{l0} - \mathrm{i}\eta]} \right.$$

$$+\frac{[\hat{\rho}(\mathbf{r}_2)]_{0n}\,[\hat{\rho}(\mathbf{r}_1)]_{nl}\,[\hat{\rho}(\mathbf{r}_3)]_{l0}}{[\omega'-\omega_{n0}-\mathrm{i}\eta]\,[\omega''+\omega_{l0}-\mathrm{i}\eta]}+\frac{[\hat{\rho}(\mathbf{r}_3)]_{0n}\,[\hat{\rho}(\mathbf{r}_2)]_{nl}\,[\hat{\rho}(\mathbf{r}_1)]_{l0}}{[\omega''-\omega_{n0}-\mathrm{i}\eta]\,[\omega+\omega_{l0}+\mathrm{i}\eta]}$$
$$+\frac{[\hat{\rho}(\mathbf{r}_1)]_{0n}\,[\hat{\rho}(\mathbf{r}_2)]_{nl}\,[\hat{\rho}(\mathbf{r}_3)]_{l0}}{[\omega-\omega_{n0}+\mathrm{i}\eta]\,[\omega''+\omega_{l0}-\mathrm{i}\eta]}+\frac{[\hat{\rho}(\mathbf{r}_3)]_{0n}\,[\hat{\rho}(\mathbf{r}_1)]_{nl}\,[\hat{\rho}(\mathbf{r}_2)]_{l0}}{[\omega''-\omega_{n0}-\mathrm{i}\eta]\,[\omega'+\omega_{l0}-\mathrm{i}\eta]}$$
$$+\frac{[\hat{\rho}(\mathbf{r}_2)]_{0n}\,[\hat{\rho}(\mathbf{r}_3)]_{nl}\,[\hat{\rho}(\mathbf{r}_1)]_{l0}}{[\omega'-\omega_{n0}-\mathrm{i}\eta]\,[\omega+\omega_{l0}+\mathrm{i}\eta]}\Bigg]. \tag{5}$$

Here, Ω is the normalization volume, $\hat{\rho}(\mathbf{r})$ is the particle-density operator, and $[\hat{\rho}(\mathbf{r})]_{nl}$ are matrix elements taken between the exact many-electron states Ψ_n and Ψ_l of energy E_n and E_l. Φ_0 and E_0 represent the exact many-electron ground state and energy, respectively, $\omega_{nl}=E_n-E_l$, $\omega''=-(\omega+\omega')$, and η is a positive infinitesimal.

The total energy lost by the probe particle is simply

$$-\Delta E=\int_{-\infty}^{+\infty}dt\left(-\frac{dE}{dt}\right), \tag{6}$$

which can also be obtained by first considering the probability $P_{\mathbf{q},\omega}$ for the probe particle to transfer momentum $\mathbf{q}$ and energy ω to the many-electron system and then multiplying $P_{\mathbf{q},\omega}$ by the energy transfer ω and summing over all $\mathbf{q}$ and ω [29, 43, 44, 45].

The many-body ground and excited states of a many-electron system are *unknown*; hence, the exact linear and quadratic density-response functions are difficult to calculate. In the framework of time-dependent density functional theory [TDDFT] [46], the exact density-response functions are obtained from the knowledge of their noninteracting counterparts and the exchange-correlation (xc) kernel $f_{xc}(\mathbf{r},\mathbf{r}',\omega)$ which equals the second functional derivative of the *unknown* xc energy functional $E_{xc}[n]$. In the so-called time-dependent Hartree approximation or RPA, the xc kernel is simply taken to be zero.

In the case of a noninteracting Fermi gas, the ground state is obtained by simply filling all the single-particle states of noninteracting electrons below the Fermi level. When acting on the ground state, the particle-density operator $\hat{\rho}(\mathbf{r})$ produces single-particle transitions in which a given particle is scattered from some state inside the Fermi sea to a state outside. Hence, the linear and quadratic density-response functions of Eqs. (4) and (5) reduce to

their noninteracting counterparts:

$$\chi^0(\mathbf{r}_1,\mathbf{r}_2;\omega)=\frac{2}{\Omega}\sum_{i,j}f_i\left[\frac{\phi_i(\mathbf{r}_1)\phi_j^*(\mathbf{r}_1)\phi_j(\mathbf{r}_2)\phi_i^*(\mathbf{r}_2)}{\omega-\omega_{ji}+\mathrm{i}\eta}-\frac{\phi_i(\mathbf{r}_2)\phi_j^*(\mathbf{r}_2)\phi_j(\mathbf{r}_1)\phi_i^*(\mathbf{r}_1)}{\omega+\omega_{ji}+\mathrm{i}\eta}\right] \tag{7}$$

and

$$\begin{aligned}Y^0(\mathbf{r}_1,\mathbf{r}_2,\mathbf{r}_3;\omega,\omega')=-\frac{1}{\Omega}\sum_{i,j,k}f_i\Bigg[&\frac{\phi_i(\mathbf{r}_1)\phi_j^*(\mathbf{r}_1)\phi_j(\mathbf{r}_3)\phi_k^*(\mathbf{r}_3)\phi_k(\mathbf{r}_2)\phi_i^*(\mathbf{r}_2)}{[\omega-\omega_{ji}+\mathrm{i}\eta]\,[\omega'+\omega_{ki}-\mathrm{i}\eta]}\\
+&\frac{\phi_i(\mathbf{r}_2)\phi_j^*(\mathbf{r}_2)\phi_j(\mathbf{r}_1)\phi_k^*(\mathbf{r}_1)\phi_k(\mathbf{r}_3)\phi_i^*(\mathbf{r}_3)}{[\omega'-\omega_{ji}-\mathrm{i}\eta]\,[\omega''+\omega_{ki}-\mathrm{i}\eta]}+\frac{\phi_i(\mathbf{r}_3)\phi_j^*(\mathbf{r}_3)\phi_j(\mathbf{r}_2)\phi_k^*(\mathbf{r}_2)\phi_k(\mathbf{r}_1)\phi_i^*(\mathbf{r}_1)}{[\omega''-\omega_{ji}-\mathrm{i}\eta]\,[\omega+\omega_{ki}+\mathrm{i}\eta]}\\
+&\frac{\phi_i(\mathbf{r}_1)\phi_j^*(\mathbf{r}_1)\phi_j(\mathbf{r}_2)\phi_k^*(\mathbf{r}_2)\phi_k(\mathbf{r}_3)\phi_i^*(\mathbf{r}_3)}{[\omega-\omega_{ji}+\mathrm{i}\eta]\,[\omega''+\omega_{ki}-\mathrm{i}\eta]}+\frac{\phi_i(\mathbf{r}_3)\phi_j^*(\mathbf{r}_3)\phi_j(\mathbf{r}_1)\phi_k^*(\mathbf{r}_1)\phi_k(\mathbf{r}_2)\phi_i^*(\mathbf{r}_2)}{[\omega''-\omega_{ji}-\mathrm{i}\eta]\,[\omega'+\omega_{ji}-\mathrm{i}\eta]}\\
+&\frac{\phi_i(\mathbf{r}_2)\phi_j^*(\mathbf{r}_2)\phi_j(\mathbf{r}_3)\phi_k^*(\mathbf{r}_3)\phi_k(\mathbf{r}_1)\phi_i^*(\mathbf{r}_1)}{[\omega'-\omega_{ji}-\mathrm{i}\eta]\,[\omega+\omega_{ki}+\mathrm{i}\eta]}\Bigg],\end{aligned} \tag{8}$$

where $\omega_{ji}=\varepsilon_j-\varepsilon_i$, and f_i are Fermi-Dirac occupation factors. At zero temperature $f_i=\Theta(\varepsilon_F-\varepsilon_i)$, ε_F being the Fermi energy, and $\Theta(x)$, the Heaviside step function. The single-particle states $\phi_i(\mathbf{r})$ and energies ε_i entering Eqs. (7) and (8) are usually chosen to be the eigenfunctions and eigenvalues of an effective Hartree [47], Kohn-Sham [48], or quasiparticle [49, 50] hamiltonian [51].

In the RPA, the induced potential $V^{ind}(\mathbf{r},t)$ is simply obtained as the potential induced in a noninteracting Fermi system by both the probe-particle charge density $\rho^{ext}(\mathbf{r},t)$ and the induced electron density $\rho^{ind}(\mathbf{r},t)$, i.e.,

$$\begin{aligned}V^{ind}(\mathbf{r},t) &= \int d\mathbf{r}'\int_{-\infty}^{+\infty}dt'\int_{-\infty}^{+\infty}\frac{d\omega}{2\pi}\,\mathrm{e}^{-i\omega(t-t')}\int d\mathbf{r}_1\int d\mathbf{r}_3\,v(\mathbf{r},\mathbf{r}_1)\\
&\times \Bigg\{\chi^0(\mathbf{r}_1,\mathbf{r}_3;\omega)+\int d\mathbf{r}''\int_{-\infty}^{+\infty}dt''\int_{-\infty}^{+\infty}\frac{d\omega'}{2\pi}\mathrm{e}^{-i(\omega+\omega')(t'-t'')}\\
&\times \int d\mathbf{r}_2\,Y^0(\mathbf{r}_1,\mathbf{r}_2,\mathbf{r}_3;\omega,\omega')\,v(\mathbf{r}_2,\mathbf{r}'')\,\left[\rho^{ext}(\mathbf{r}'',t'')+\rho^{ind}(\mathbf{r}'',t'')\right]\Bigg\}\\
&\times v(\mathbf{r}_3,\mathbf{r}')\,\left[\rho^{ext}(\mathbf{r}',t')+\rho^{ind}(\mathbf{r}',t')\right].\end{aligned} \tag{9}$$

Assuming that

$$V^{ind}(\mathbf{r},t)=\int d\mathbf{r}'\,v(\mathbf{r},\mathbf{r}')\rho^{ind}(\mathbf{r}',t), \tag{10}$$

one easily finds that the induced potential $V^{ind}(\mathbf{r},t)$ of Eq. (9) is of the form of Eq. (3) with the exact interacting linear and quadratic density-response functions being replaced by the following integral equations:

$$\chi(\mathbf{r},\mathbf{r}';\omega) = \chi^0(\mathbf{r},\mathbf{r}';\omega) + \int d\mathbf{r}_1 \int d\mathbf{r}_2 \chi^0(\mathbf{r},\mathbf{r}_1;\omega) v(\mathbf{r}_1,\mathbf{r}_2) \chi(\mathbf{r}_2,\mathbf{r}';\omega) \quad (11)$$

and

$$\begin{aligned} Y(\mathbf{r},\mathbf{r}',\mathbf{r}'';\omega,\omega') &= \int d\mathbf{r}_1 \int d\mathbf{r}_2 \int d\mathbf{r}_3 K(\mathbf{r},\mathbf{r}_1;\omega) Y^0(\mathbf{r}_1,\mathbf{r}_2,\mathbf{r}_3;\omega,\omega') \\ &\times K(\mathbf{r}_2,\mathbf{r}';-\omega') K(\mathbf{r}_3,\mathbf{r}'';\omega+\omega'), \end{aligned} \quad (12)$$

where $K(\mathbf{r},\mathbf{r}';\omega)$ is the so-called inverse dielectric function

$$K(\mathbf{r},\mathbf{r}';\omega) = \delta(\mathbf{r}-\mathbf{r}') + \int d\mathbf{r}_1 \, \chi(\mathbf{r},\mathbf{r}_1;\omega) \, v(\mathbf{r}_1,\mathbf{r}'). \quad (13)$$

2.1 Uniform electron gas

In the case of a uniform FEG, there is translational invariance in all directions. Hence, Eq. (6) yields

$$-\Delta E = L \left(-\frac{dE}{dx}\right), \quad (14)$$

where L is the normalization length, and $(-dE/dx)$ is the energy loss per unit path length of the projectile, i.e., the so-called stopping power of the electron system:

$$\begin{aligned} -\frac{dE}{dx} &= 4\pi Z_1^2 \int \frac{d\mathbf{q}}{(2\pi)^3} \int_0^\infty \frac{d\omega}{2\pi} \, \omega \, v_{\mathbf{q}} \, \delta(\omega - \mathbf{q}\cdot\mathbf{v}) \\ &\times \left[-\mathrm{Im} K_{\mathbf{q},\omega} + 2\pi Z_1 \int \frac{d\mathbf{q}_1}{(2\pi)^4} \int_{-\infty}^\infty \frac{d\omega_1}{2\pi} \, \mathrm{Im} Y_{\mathbf{q},\omega;-\mathbf{q}_1,-\omega_1} \, v_{\mathbf{q}_1} \, v_{\mathbf{q}-\mathbf{q}_1} \, \delta\left(\omega_1^0 - \mathbf{q}_1\cdot\mathbf{v}\right) \right], \end{aligned} \quad (15)$$

$v_{\mathbf{q}} = 4\pi/q^2$, $K_{\mathbf{q},\omega}$, and $Y_{\mathbf{q}_1,\omega_1;\mathbf{q}_2,\omega_2}$ being Fourier transforms of the bare Coulomb interaction $v(\mathbf{r},\mathbf{r}')$, the inverse dielectric function $K(\mathbf{r},\mathbf{r}',\omega)$, and the quadratic density-response function $Y(\mathbf{r},\mathbf{r}',\mathbf{r}'';\omega,\omega')$, respectively.

In the RPA,

$$K_{\mathbf{q},\omega} = 1 + \chi_{\mathbf{q},\omega} \, v_{\mathbf{q}}, \quad (16)$$

$$\chi_{\mathbf{q},\omega} = \chi^0_{\mathbf{q},\omega} + \chi^0_{\mathbf{q},\omega}\, v_{\mathbf{q}}\, \chi_{\mathbf{q},\omega}, \tag{17}$$

and

$$Y_{\mathbf{q}_1,\mathbf{q}_2;\omega_1,\omega_2} = K_{\mathbf{q}_1,\omega_1}\, Y^0_{\mathbf{q}_1,\mathbf{q}_2;\omega_1,\omega_2}\, K_{-\mathbf{q}_1,-\omega_1}\, K_{\mathbf{q}_1+\mathbf{q}_2,\omega_1+\omega_2}, \tag{18}$$

$\chi^0_{\mathbf{q},\omega}$ and $Y^0_{\mathbf{q}_1,\mathbf{q}_2;\omega_1,\omega_2}$ being Fourier transforms of the noninteracting linear and quadratic density-response functions $\chi^0(\mathbf{r}_1,\mathbf{r}_2;\omega)$ and $Y^0(\mathbf{r}_1,\mathbf{r}_2,\mathbf{r}_3;\omega,\omega')$ [see Eqs. (7) and (8)]. Noting that for a uniform electron gas the single-particle states $\phi_i(\mathbf{r})$ entering Eqs. (7) and (8) are simply plane waves of the form

$$\phi_{\mathbf{k}}(\mathbf{r}) = \frac{1}{\sqrt{\Omega}} \mathrm{e}^{i\mathbf{k}\cdot\mathbf{r}}, \tag{19}$$

analytic expressions for both $\chi^0_{\mathbf{q},\omega}$ and $Y^0_{\mathbf{q}_1,\mathbf{q}_2;\omega_1,\omega_2}$ can be obtained. $\chi^0_{\mathbf{q},\omega}$ is the Lindhard function [6, 47]. Explicit expressions for the real and imaginary parts of the noninteracting quadratic density-response function $Y^0_{\mathbf{q}_1,\mathbf{q}_2;\omega_1,\omega_2}$ where reported in Refs. [52] and [16, 29], respectively, and an extension to imaginary frequencies was later reported in Ref. [53].

2.1.1 High-velocity limit

For high projectile velocities, the zero-point motion of the electron gas can be neglected and it can be considered, therefore, as if it were at rest. Thus, in this approximation all energies ε_i entering Eqs. (7) and (8) can be set equal to zero. If one further assumes that $v^2 >> \omega_p$, ω_p being the plasmon frequency for which $K_{0,\omega}$ diverges, Eq. (15) is found to yield [29]

$$-\frac{dE}{dx} \approx \frac{4\pi n Z_1^2}{v^2}(L_0 + Z_1 L_1), \tag{20}$$

where

$$L_0 = \ln \frac{2v^2}{\omega_p} \tag{21}$$

and

$$L_1 = 1.42 \frac{\pi\omega_p}{v^3} \ln \frac{2v^2}{2.13\omega_p}, \tag{22}$$

n being the density of free electrons in the target. The first term, which for a relatively low projectile charge Z_1 gives the main contribution to the stopping power, is proportional to Z_1^2 and has the same form as the Bethe formula for the inelastic stopping power of atoms [4] as long as the plasma

frequency ω_p is replaced by the mean excitation energy of electrons in the atom. The second term, which originates the so-called Barkas effect, i.e., the dependence of the stopping power on the sign of the projectile charge, has been found to yield excellent agreement with stopping-power measurements at high velocities [16, 54].

2.1.2 Double-plasmon excitation

In the RPA, the linear-response contribution to the stopping power of Eq. (15), which is proportional to Z_1^2, is fully originated in the creation of single e-h pairs and plasmons. Furthermore, the contribution to the actual (beyond RPA) Z_1^2 stopping power that is due to coherent multiple excitations such as double plasmons is expected to be relatively small. Nevertheless, accurate measurements of electron energy-loss spectra showed evidence for the existence of coherent double-plasmon excitations [17, 18].

In the framework of many-body perturbation theory, one first defines the scattering matrix S as a time-ordered exponential in terms of the perturbing hamiltonian and field operators [47]. Then, one considers the matrix elements corresponding to the process in which the recoiless probe particle carries the system either from an initial state $a_i^+\Phi_0$ to a final state $a_f\Phi_0$ (single excitation) or from an initial state $a_{i_1}^+a_{i_2}^+\Phi_0$ to a final state $a_{f_1}^+a_{f_2}^+\Phi_0$ (double excitation):

$$S_{f,i} = \frac{<\Phi_0|a_f S a_i^+|\Phi_0>}{<\Phi_0|S|\Phi_0>} \tag{23}$$

and

$$S_{f_1,f_2;i_1,i_2} = \frac{<\Phi_0|a_{f_1}a_{f_2}S a_{i_1}^+a_{i_2}^+|\Phi_0>}{<\Phi_0|S|\Phi_0>}, \tag{24}$$

where a_i and a_i^+ are annihilation and creation operators, respectively, and Φ_0 represents the vacuum state. Finally, one calculates the probability for the probe particle to transfer momentum $\mathbf{q}$ and energy ω to the many-electron system by moving either one, two, or more particles from inside the Fermi sea to outside:

$$\begin{aligned} P_{\mathbf{q},\omega} &= 2\sum_{\mathbf{s}} f_{\mathbf{s}} \sum_{\mathbf{p}} (1-f_{\mathbf{p}}) \left|S_{f,i}\right|^2 \delta^4_{q,p-s} + 4\sum_{\mathbf{q}_1}\sum_{\omega_1}\sum_{\mathbf{s}_1} f_{\mathbf{s}_1} \sum_{\mathbf{s}_2} f_{\mathbf{s}_2} \sum_{\mathbf{p}_1}(1-f_{\mathbf{p}_1}) \\ &\times \sum_{\mathbf{p}_2}(1-f_{\mathbf{p}_2}) \left|S_{f_1,f_2;i_1,i_2}\right|^2 \delta^4_{q_1,p_1-s_1}\delta^4_{q-q_1,p_2-s_2} + \cdots, \end{aligned} \tag{25}$$

$\delta^4_{q,q'} = \delta^3_{\mathbf{q},\mathbf{q}'}\delta_{\omega,\omega'}$ being the symmetric Kronecker δ symbol. If the probe-particle is not a heavy particle, energy conservation should be ensured by introducing recoil into the argument of the delta functions. If the probe is an electron, a step function should also be introduced to ensure that the probe electron does not lose enough energy to fall below the Fermi level.

The stopping power of the electron system is obtained by first multiplying the probability $P_{\mathbf{q},\omega}$ of Eq. (25) by the energy transfer ω and then summing over all $\mathbf{q}$ and ω:

$$-\frac{dE}{dx} = \frac{1}{L}\sum_{\mathbf{q}}\sum_{\omega}\omega\, P_{\mathbf{q},\omega}. \tag{26}$$

A careful analysis of the various contributions to the probability $P_{\mathbf{q},\omega}$ that are proportional to Z_1^2 and Z_1^3 yields, to third order in the RPA screened interaction $v_{\mathbf{q}}\, K_{\mathbf{q},\omega}$, an expression for the stopping power that exactly coincides with Eq. (15) [44]. Alternatively, the inverse mean free path is obtained as follows

$$\lambda^{-1} = \frac{1}{L}\sum_{\mathbf{q}}\sum_{\omega} P_{\mathbf{q},\omega}. \tag{27}$$

The lowest-order Z_1^2 contribution to the probability $P^{2p}_{\mathbf{q},\omega}$ for a probe-electron ($Z_1 = -1$) to excite a double plasmon, which is of fourth order in the RPA screened interaction $v_{\mathbf{q}}K_{\mathbf{q},\omega}$, is found to be given by the following expression:

$$\begin{aligned} P^{2p}_{\mathbf{q},\omega} &= 16\pi Z_1^2\, v_{\mathbf{q}}^{-2} K^{-2}_{\mathbf{q},\omega} \sum_{\mathbf{q}_1} v_{\mathbf{q}_1} v_{\mathbf{q}-\mathbf{q}_1} \int_0^{\omega} \frac{d\omega_1}{2\pi}\, \mathrm{Im}K_{\mathbf{q}_1,\omega_1}\, \mathrm{Im}K_{\mathbf{q}-\mathbf{q}_1,\omega-\omega_1} \\ &\times \; |Y_{\mathbf{q},\mathbf{q}_1;\omega,\omega_1}|^2\, \delta(q^0 - p^0 + \omega_{\mathbf{v}-\mathbf{q}})\, \Theta(\omega_{\mathbf{v}-\mathbf{q}} - \varepsilon_F), \end{aligned} \tag{28}$$

where $\omega_{\mathbf{k}} = k^2/2$. If one approximates both the linear and quadratic density-response functions entering Eq. (28) by their low-$\mathbf{q}$ limits, one only keeps the high-velocity limit of this probability in an expansion in terms of the inverse velocity, and one introduces this limit into Eq. (27), one obtains the following result for the Z_1^2 contribution to the inverse mean free path that is due to the excitation of a double plasmon [20, 55]:

$$\lambda^{-1}_{2p} \approx 0.164\, Z_1^2\, \frac{\sqrt{r_s}}{36\pi v^2}, \tag{29}$$

r_s being the so-called electron-density parameter r_s defined by the relation $1/n = (4\pi/3)(r_s\, a_0)^3$. Numerical study shows [21] that introduction of the

full RPA linear and quadratic density-response functions into Eq. (28) yields a result for λ_{2p}^{-1} which has, in the high-velocity limit, the same velocity dependence as the approximation of Eq. (29), though for $r_s = 2.07$ the full RPA λ_{2p}^{-1} is found to be larger than this approximation by a factor of 2.16.

2.2 Bounded electron gas

In the case of charged particles moving inside a solid, nonlinear effects are known to be crucial in the interpretation of energy-loss measurements. However, these corrections have been shown to be less important when the charged particle moves outside the solid [56]. Hence, in the case of a bounded three-dimensional electron gas we restrict the calculations to linear-response theory. Assuming translational invariance in two directions, which we take to be normal to the z axis, to first order in the external perturbation (linear-response theory) the energy loss of Eq. (6) may be expressed as follows [57]

$$\begin{aligned} -\Delta E &= -\frac{Z_1^2}{\pi}\int \frac{d\mathbf{q}_\parallel}{(2\pi)^2}\int_{-\infty}^{+\infty} dt \int_{-\infty}^{+\infty} dt' \int_0^{\infty} d\omega\, \omega \\ &\times \mathrm{e}^{-i(\omega-\mathbf{q}_\parallel\cdot\mathbf{v}_\parallel)(t-t')}\,\mathrm{Im}W[z(t),z(t');\mathbf{q}_\parallel,\omega], \end{aligned} \tag{30}$$

where $\mathbf{q}_\parallel$ and $\mathbf{v}_\parallel$ are components of the momentum transfer and the velocity in the plane of the surface, $z(t)$ represents the position of the projectile relative to the surface, and

$$W(z,z';\mathbf{q}_\parallel,\omega) = v(z,z',\mathbf{q}_\parallel) + \int dz_1 \int dz_2\, v(z,z_1;\mathbf{q}_\parallel)\,\chi(z_1,z_2;\mathbf{q}_\parallel,\omega)\,v(z_2,z';\mathbf{q}_\parallel), \tag{31}$$

$v(z,z';\mathbf{q}_\parallel) = (2\pi/q_\parallel)\mathrm{e}^{-q_\parallel|z-z'|}$ and $\chi(z,z';\mathbf{q}_\parallel,\omega)$ being two-dimensional Fourier transforms of the bare Coulomb interaction and the density-response function, respectively.

In the RPA,

$$\begin{aligned} \chi(z,z';\mathbf{q}_\parallel,\omega) &= \chi^0(z,z';\mathbf{q}_\parallel,\omega) + \int dz_1 \int \mathrm{d}z_2 \chi^0(z,z_1;\mathbf{q}_\parallel,\omega) \\ &\times v(z_1,z_2;\mathbf{q}_\parallel)\,\chi(z_2,z';\mathbf{q}_\parallel,\omega), \end{aligned} \tag{32}$$

where

$$\chi^0(z,z';\mathbf{q}_\parallel,\omega) = 2\sum_{i,j}\phi_i(z)\phi_j^*(z)\phi_j(z')\phi_i^*(z')\int \frac{\mathrm{d}\mathbf{k}_\parallel}{(2\pi)^2}\,\frac{f_i-f_j}{E_i-E_j+(\omega+i\eta)}. \tag{33}$$

Here,

$$E_i = \varepsilon_i + \frac{\mathbf{k}_\parallel^2}{2} \tag{34}$$

and

$$E_j = \varepsilon_j + \frac{(\mathbf{k}_\parallel + \mathbf{q}_\parallel)^2}{2}, \tag{35}$$

the wave functions $\phi_i(z)$ and energies ε_i, which describe motion normal to the surface, being the eigenfunctions and eigenvalues of a one-dimensional Hartree, Kohn-Sham, or quasiparticle hamiltonian.

Eq. (30) gives the energy that a charged particle moving with constant velocity along an arbitrary trajectory loses due to electronic excitations in an electron system that is translationally invariant in two directions, as occurs in the case of a simple metal surface modeled by jellium.

2.2.1 Parallel trajectory

In the glancing incidence geometry ions penetrate into the material, they skim the outermost layer of the solid, and are then repelled by a repulsive, screened Coulomb potential, as discussed by Gemmell [58]. Through use of the appropriate effective potentials the ion trajectory $z(t)$ can be calculated and the energy loss is then obtained from Eq. (30). Under extreme grazing-incidence conditions, incident charged particles can be assumed to move with constant velocity $\mathbf{v}$ along a definite trajectory at a fixed distance z from a jellium surface. Eq. (30) then yields Eq. (14), as in the case of charged particles moving in a uniform electron gas, but with the energy loss per unit path length now being given by the following expression [57]:

$$-\frac{dE}{dx} = -\frac{2}{v} Z_1^2 \int \frac{d\mathbf{q}_\parallel}{(2\pi)^2} \int_0^\infty d\omega\, \omega\, \mathrm{Im} W(z, z; \mathbf{q}_\parallel, \omega)\, \delta(\omega - \mathbf{q}_\parallel \cdot \mathbf{v}). \tag{36}$$

2.2.2 High-velocity limit

At high velocities, the energy-loss spectrum for charged particles moving outside a solid is known to be dominated by long-wavelength ($q_\parallel \to 0$) surface-plasmon excitations [59]. In this long-wavelength limit, the imaginary part of Eq. (31) yields [60]

$$\mathrm{Im}\, W(z, z'; q_\parallel, \omega) = -\frac{\pi^2}{q_\parallel} e^{-q_\parallel (z+z')}\, \omega_s\, \delta(\omega - \omega_s), \tag{37}$$

where $\omega_s = \omega_p/\sqrt{2}$, $\omega_p = (4\pi n)^{1/2}$ being the classical plasma frequency of a uniform electron gas of density n.

Introducing Eq. (37) into Eq. (36), one easily reproduces the classical expression of Echenique and Pendry [61]:

$$-\frac{dE}{dx} = Z_1^2 \, \frac{\omega_s^2}{v^2} \, \mathrm{K}_0(2\,\omega_s\, z/v), \tag{38}$$

where K_0 is the zero-order modified Bessel function. For large values of z ($z >> v/\omega_s$), Eq. (38) reduces to

$$-\frac{dE}{dx} = Z_1^2 \, \frac{\omega_s}{2\,v} \, \sqrt{\pi\,\omega_s/z\,v} \; e^{-2\,\omega_s\, z/v}. \tag{39}$$

2.3 Periodic crystals

For a peridic crystal, we introduce the following Fourier expansion of the linear density-response function:

$$\chi(\mathbf{r},\mathbf{r}';\omega) = \frac{1}{\Omega} \sum_{\mathbf{q}}^{BZ} \sum_{\mathbf{G},\mathbf{G}'} \mathrm{e}^{\mathrm{i}(\mathbf{q}+\mathbf{G})\cdot\mathbf{r}} \mathrm{e}^{-\mathrm{i}(\mathbf{q}+\mathbf{G}')\cdot\mathbf{r}'} \chi_{\mathbf{G},\mathbf{G}'}(\mathbf{q},\omega), \tag{40}$$

where the first sum runs over $\mathbf{q}$ vectors within the first Brillouin zone (BZ), and $\mathbf{G}$ and $\mathbf{G}'$ are reciprocal lattice vectors.

In the RPA,

$$\chi_{\mathbf{G},\mathbf{G}'}(\mathbf{q},\omega) = \chi^0_{\mathbf{G},\mathbf{G}'}(\mathbf{q},\omega) + \sum_{\mathbf{G}''} \chi^0_{\mathbf{G},\mathbf{G}''}(\mathbf{q},\omega) v_{\mathbf{q}+\mathbf{G}''} \, \chi_{\mathbf{G}'',\mathbf{G}'}(\mathbf{q},\omega), \tag{41}$$

where $v_{\mathbf{q}+\mathbf{G}}$ and $\chi^0_{\mathbf{G},\mathbf{G}'}(\mathbf{q},\omega)$ represent the Fourier coefficients of the bare Coulomb interaction $v(\mathbf{r},\mathbf{r}')$ and the noninteracting density-response function $\chi^0(\mathbf{r},\mathbf{r}';\omega)$, respectively:

$$v_{\mathbf{q}+\mathbf{G}} = \frac{4\pi}{|\mathbf{q}+\mathbf{G}|^2} \tag{42}$$

and

$$\begin{aligned} \chi^0_{\mathbf{G},\mathbf{G}'}(\mathbf{q},\omega) &= \frac{1}{\Omega} \sum_{\mathbf{k}}^{BZ} \sum_{n,n'} (f_{\mathbf{k},n} - f_{\mathbf{k}+\mathbf{q},n'}) \\ &\times \frac{\langle \phi_{\mathbf{k},n} | e^{-\mathrm{i}(\mathbf{q}+\mathbf{G})\cdot\mathbf{r}} | \phi_{\mathbf{k}+\mathbf{q},n'} \rangle \langle \phi_{\mathbf{k}+\mathbf{q},n'} | e^{\mathrm{i}(\mathbf{q}+\mathbf{G}')\cdot\mathbf{r}} | \phi_{\mathbf{k},n} \rangle}{E_{\mathbf{k},n} - E_{\mathbf{k}+\mathbf{q},n'} + \hbar(\omega + \mathrm{i}\eta)}, \end{aligned} \tag{43}$$

$\phi_{\mathbf{k},n}$ and $E_{\mathbf{k},n}$ being Bloch eigenfunctions and eigenvalues of a three-dimensional Hartree, Kohn-Sham, or quasiparticle hamiltonian.

The stopping power of a periodic crystal is obtained by first introducing Eqs. (2) and (3) into Eq. (1), and then introducing Eq. (1) into Eq. (6). Within linear-response theory, i.e., to first order in the external perturbation, the result is of the form of Eq. (14) with the energy loss per unit path length being given by the following expression:

$$\left[-\frac{dE}{dx}\right]_{\mathbf{b}} = -\frac{2\,Z_1^2}{v\,\Omega}\sum_{\mathbf{q}}^{\mathrm{BZ}}\sum_{\mathbf{G}}\sum_{\mathbf{G}'_\perp}\omega\,\mathrm{e}^{\mathrm{i}\mathbf{G}'_\perp\cdot\mathbf{b}}\,v_{\mathbf{q}+\mathbf{G}+\mathbf{G}'_\perp}\,\mathrm{Im}\,K_{\mathbf{G},\mathbf{G}+\mathbf{G}'_\perp}(\mathbf{q},\omega), \qquad (44)$$

where $\mathbf{b}$ is the impact vector of the projectile, the sum $\sum_{\mathbf{G}'_\perp}$ is restricted to those reciprocal-lattice vectors that are perpendicular to the projectile velocity ($\mathbf{G}'_\perp\cdot\mathbf{v}=0$), $\omega=(\mathbf{q}+\mathbf{G})\cdot\mathbf{v}$, and $K_{\mathbf{G},\mathbf{G}'}(\mathbf{q},\omega)$ represent the Fourier coefficients of the inverse dielectric function $K(\mathbf{r},\mathbf{r}';\omega)$:

$$K_{\mathbf{G},\mathbf{G}'}(\mathbf{q},\omega) = \delta_{\mathbf{G},\mathbf{G}'} + v_{\mathbf{q}+\mathbf{G}}\,\chi_{\mathbf{G},\mathbf{G}'}(\mathbf{q},\omega). \qquad (45)$$

The stopping power of Eq. (44) is the so-called position-dependent stopping power. The most important contribution to this quantity is provided by the term $\mathbf{G}'_\perp=0$, the magnitude of the other terms depending on the direction of the velocity. For a few highly symmetric or *channeling* directions non-negligible corrections to the $\mathbf{G}'_\perp=0$ contribution are found, thus exhibiting the characteristic anisotropy of the position-dependent stopping power. However, for those directions for which the condition of $\mathbf{G}'_\perp\cdot\mathbf{v}=0$ is never satisfied only the $\mathbf{G}'_\perp=0$ term contributes and one finds

$$\left[-\frac{dE}{dx}\right]_{\mathrm{random}} = -\frac{2\,Z_1^2}{v\,\Omega}\sum_{\mathbf{q}}^{\mathrm{BZ}}\sum_{\mathbf{G}}\omega\,v_{\mathbf{q}+\mathbf{G}}\,\mathrm{Im}\,K_{\mathbf{G},\mathbf{G}}(\mathbf{q},\omega). \qquad (46)$$

This is the so-called random stopping power, which is also obtained as the average over impact parameters of the position-dependent stopping power of Eq. (44). For simple metals like Al the diagonal elements of the inverse dielectric matrix $K_{\mathbf{G},\mathbf{G}}(\mathbf{q},\omega)$ are rather isotropic, in which case there is little dependence of the random stopping power on the direction of the projectile velocity.

3 Results

In this section, we review existing calculations of the stopping power of both an infinite (uniform) and a semi-infinite (bounded) free gas of interacting electrons, double-plasmon inverse mean free paths, and the linear (lowest-order) first-principles stopping power of real Al and Si. New calculations of the various contributions to the stopping power due to the excitation of e-h pairs and plasmons are also reported, existing double-plasmon calculations are extended to low velocities where both recoil and the probe-particle statistics play a role, and existing first-principles calculations of the stopping power of Al and Si are extended by allowing transitions with large values of the momentum transfer.

3.1 Uniform electron gas

Here we consider a uniform gas of interacting electrons, the electron density n being equal to the average electron density of valence electrons in aluminum metal ($r_s = 2.07$), for which the Fermi momentum [$q_F = (3\pi^2 n)^{1/3}$] and bulk plasma frequency [$\omega_p = (4\pi n)^{1/2}$] are $q_F = 0.927\, a_0^{-1}$ and $\omega_p = 15.8$ eV, respectively. We set $Z_1 = 1$ (probe bare protons) for the stopping-power calculations and $Z_1 = -1$ (probe electrons) for the calculations of the double-plasmon inverse mean free path. Our results can then be easily extended to arbitrary values of Z_1, as linear and quadratic contributions to the stopping power and the inverse mean free path are proportional to Z_1^2 and Z_1^3, respectively.

3.1.1 Stopping power

The second-order stopping power of a homogeneous FEG is given by Eq. (15). In Fig. 1 we show, as a function of the projectile velocity, our full RPA calculations for the separate Z_1^2 and Z_1^3 contributions to the stopping power of Eq. (15). We note that both Z_1^2 and Z_1^3 contributions to the stopping power exhibit a linear dependence on the projectile velocity up to velocities approaching the stopping maximum. This linear dependence is also exhibited by full nonlinear DFT calculations of the stopping power of a FEG [25] and by recent measurements of the electronic energy loss of protons and antiprotons [13].

The linear dependence of the Z_1^3 contribution to the stopping power is a

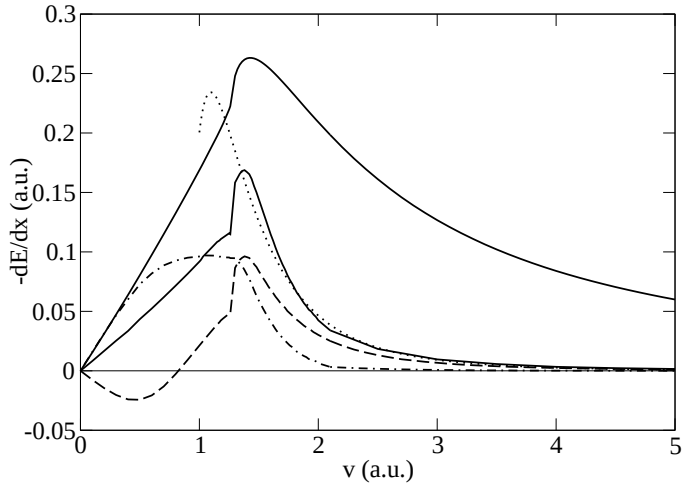

Figure 1: Solid lines represent RPA Z_1^2 and Z_1^3 contributions to the stopping power of Eq. (15), for $Z_1 = 1$ and $r_s = 2.07$, as a function of the velocity of the projectile. Dashed and dashed-dotted lines represent the RPA $[-dE/dx]^1$ and $[-dE/dx]^2$ contributions to the Z_1^3 stopping power, respectively. The dotted line is the high-velocity limit dictated by the second term of Eq. (20).

consequence of two competing effects. On the one hand, there is the effect of one-step single excitations, like those entering the Z_1^2 contribution to the stopping power, but now generated by the quadratically screened potential of the probe particle. On the other hand, there is the effect of second-order two-step single excitations generated by the linearly screened probe potential. In the RPA, these contributions to the Z_1^3 effect are given by the following expressions [29]:

$$\begin{aligned}\left[-\frac{dE}{dx}\right]^1 &= -\frac{4}{v}\,Z_1^3 \int \frac{d\mathbf{q}}{(2\pi)^3}\int_0^\infty \frac{d\omega}{2\pi}\,\omega\, v_{\mathbf{q}}\,\mathrm{Im}\,K_{\mathbf{q},\omega}\,\delta\left(\omega-\mathbf{q}\cdot\mathbf{v}\right)\int \frac{d\mathbf{q}_1}{(2\pi)^4}\int_{-\infty}^\infty \frac{d\omega_1}{2\pi} \\ &\times \mathrm{Re}\,Y^{TO}_{\mathbf{q},\omega;-\mathbf{q}_1,-\omega_1}\,v_{\mathbf{q}_1}\,\mathrm{Re}\,K_{\mathbf{q}_1,\omega_1}\,v_{\mathbf{q}-\mathbf{q}_1}\,\mathrm{Re}\,K_{\mathbf{q}-\mathbf{q}_1,\omega-\omega_1}\delta\left(\omega_1^0-\mathbf{q}_1\cdot\mathbf{v}\right)\end{aligned} \tag{47}$$

and

$$\begin{aligned}\left[-\frac{dE}{dx}\right]^2 &= -\frac{4}{v}\,Z_1^3 \int \frac{d\mathbf{q}}{(2\pi)^3}\int_0^\infty \frac{d\omega}{2\pi}\,\omega\, v_{\mathbf{q}}\,\mathrm{Re}\,K_{\mathbf{q},\omega}\,\delta\left(\omega-\mathbf{q}\cdot\mathbf{v}\right)\int \frac{d\mathbf{q}_1}{(2\pi)^4}\int_{-\infty}^\infty \frac{d\omega_1}{2\pi} \\ &\times H_{\mathbf{q},\omega;-\mathbf{q}_1,-\omega_1}\,v_{\mathbf{q}_1}\,\mathrm{Re}\,K_{\mathbf{q}_1,\omega_1}\,v_{\mathbf{q}-\mathbf{q}_1}\,\mathrm{Re}\,K_{\mathbf{q}-\mathbf{q}_1,\omega-\omega_1}\delta\left(\omega_1^0-\mathbf{q}_1\cdot\mathbf{v}\right),\end{aligned} \tag{48}$$

where $Y^{TO}_{\mathbf{q},\omega;\mathbf{q}_1,\omega_1}$ is the time-ordered counterpart of the retarded non-interacting quadratic density-response function $Y^0_{\mathbf{q},\omega;\mathbf{q}_1,\omega_1}$, and

$$H_{\mathbf{q},\omega;\mathbf{q}_1,\omega_1} = 2\pi\mathrm{sgn}(\omega)P\int \frac{\mathrm{d}^3\mathbf{k}}{(2\pi)^3} f_{\mathbf{k}}\left[\frac{\delta(\omega+\omega_{\mathbf{k}}-\omega_{\mathbf{k}+\mathbf{q}})}{\omega_1+\omega_{\mathbf{k}}-\omega_{\mathbf{k}+\mathbf{q}_1}}+\frac{\delta(\omega^0-\omega_{\mathbf{k}}+\omega_{\mathbf{k}+\mathbf{q}})}{\omega_2-\omega_{\mathbf{k}}+\omega_{\mathbf{k}+\mathbf{q}_2}}\right], \tag{49}$$

with $\mathbf{q}_2=\mathbf{q}-\mathbf{q}_1$ and $\omega_2=\omega-\omega_1$. Double excitations also contribute, within RPA, to the Z_1^3 stopping power of Eq. (15), but they are found to be zero in the low and high velocity limits and small at intermediate velocities.

The RPA $[-dE/dx]^1$ and $[-dE/dx]^2$ contributions to the stopping power of a FEG are represented in Fig. 1 by dashed and dashed-dotted lines, respectively. The $[-dE/dx]^2$ contribution from losses to two-step single excitations (dashed-dotte line) is very small at high projectile velocities where the velocity distribution of target electrons can be neglected. At high velocities, the surviving $[-dE/dx]^1$ contribution approaches the total Z_1^3 stopping power, which is very well reproduced by the second term of Eq. (20) (dotted line of Fig. 1).

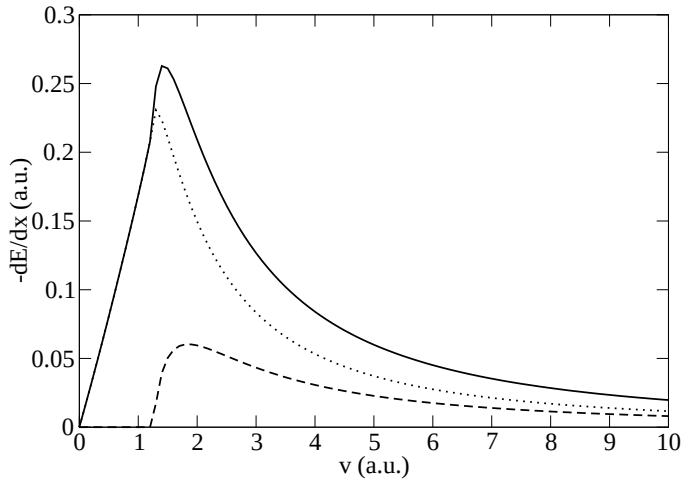

Figure 2: The solid line represents the RPA Z_1^2 (linear) contribution to the stopping power of Eq. (15), for $Z_1 = 1$ and $r_s = 2.07$, as a function of the velocity of the probe particle. Dashed and dotted lines represent contributions from the excitation of plasmons and e-h pairs, respectively.

Now we focus on the role that the excitation of e-h pairs and plasmons plays in the energy loss process. First, we restrict our calculations to the Z_1^2 (linear) contribution to the stopping power of a FEG. Fig. 2 exhibits the separate RPA e-h pair and plasmon contributions to the Z_1^2 stopping power of Eq. (15). This figure shows that the contribution from losses to plasmons is smaller for all projectile velocities than the contribution from losses to e-h pairs, which is especially true at high electron densities, although both contributions coincide in the high-velocity limit. This is the equipartition rule, which appears straightforwardly in the static-electron gas approximation. In this approximation, plasmon and e-h pair contributions to the energy loss are typically separated according to whether the momentum transfer is below ($q < q_c$) or above ($q > q_c$) the critical momentum q_c where the plasmon dispersion enters the e-h pair excitation spectrum. For an electron gas not at rest, the equipartition rule was formulated by Lindhard and Winther [62].

For a momentum transfer that is smaller than q_c, both plasmon and e-h pair excitations contribute to the full RPA energy loss, though contributions from losses due to the excitation of e-h pairs are very small. For $q > q_c$, however, only e-h pair excitations contribute. This is illustrated in Fig. 3, where

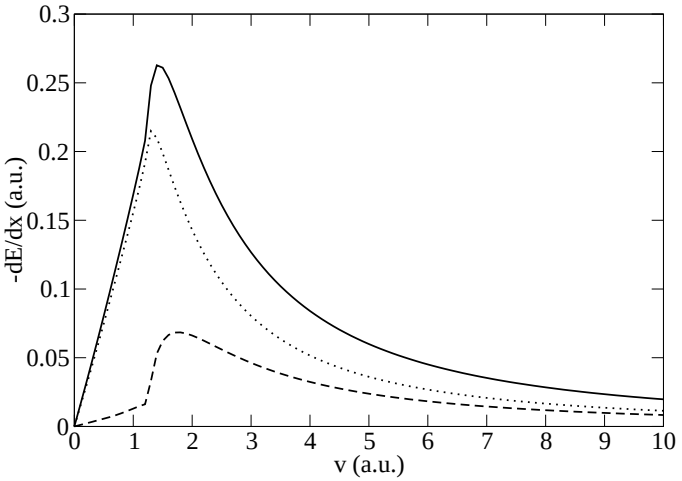

Figure 3: The solid line represents the RPA Z_1^2 (linear) contribution to the stopping power of Eq. (15), for $Z_1 = 1$ and $r_s = 2.07$, as a function of the velocity of the probe particle. Dashed and dotted lines represent contributions from momentum transfers below ($q < q_c$) and above ($q > q_c$) the critical momentum q_c where the plasmon dispersion enters the e-h pair continuum.

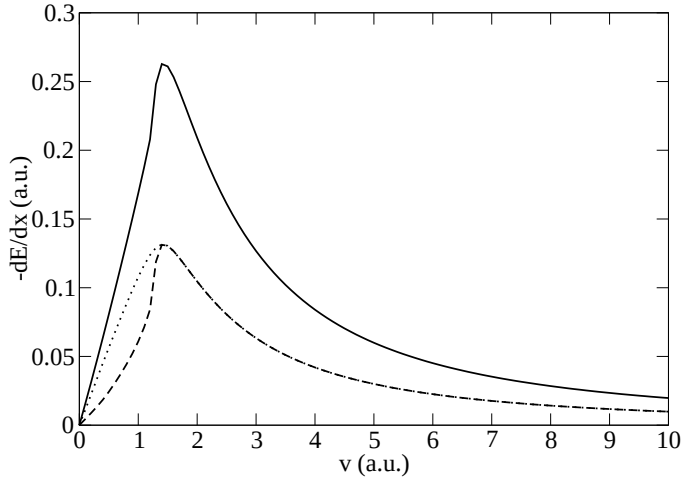

Figure 4: As in Fig. 3, but with the actual critical momentum q_c replaced by its low-density limit: $q_c \to \sqrt{2\omega_p}$.

the total Z_1^2 stopping power is separated according to whether losses correspond to momentum transfers below ($q < q_c$) or above ($q > q_c$) the critical momentum q_c. In Fig. 4, the total Z_1^2 stopping power is separated according to whether losses come from momentum transfers below ($q < \sqrt{2\omega_p}$) or above ($q > \sqrt{2\omega_p}$) the critical momentum $\sqrt{2\omega_p}$, which is the low-density limit of q_c. In this case, there is exact equipartition for all velocities above the stopping maximum. This equipartition is also found to be exact in the high-velocity limit, by using Coulomb scattering of independent electrons with $q_{\rm min} = \omega_p/v$ or by assuming that independent electrons are scatterd by a velocity-dependent Yukawa potential with screening length proportional to ω_p/v.

While the RPA $[-dE/dx]^2$ contribution to the Z_1^3 stopping power [see Eq. (48)] is entirely due to the excitation of e-h pairs, the $[-dE/dx]^1$ contribution to the Z_1^3 stopping power is originated in the excitation of both e-h pairs and plasmons. Hence, we have split $[-dE/dx]^1$ into these contributions and have found the result shown in Fig. 5 by dotted and short-dashed lines, respectively. This figure shows that contributions to the Z_1^3 effect coming from losses to plasmons is relatively smaller than in the case of the Z_1^2 term (see Fig. 2), especially at high velocities. Hence, collective excitations appear to be reasonably well described with the use of linearly screened projec-

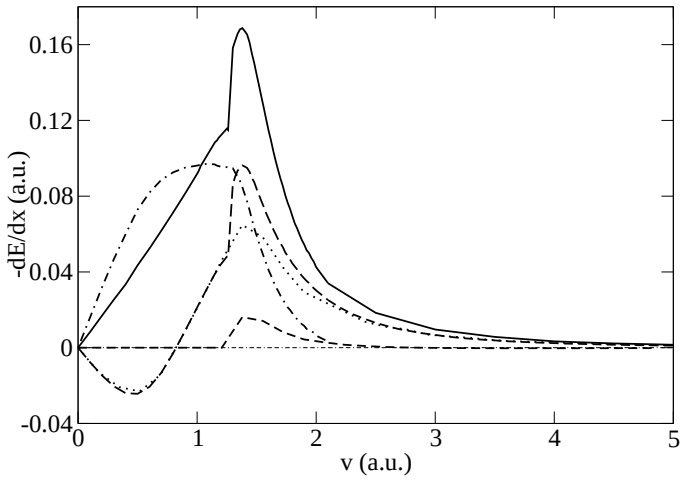

Figure 5: The solid line represents the RPA Z_1^3 (quadratic) contribution to the stopping power of Eq. (15), for $Z_1 = 1$ and $r_s = 2.07$, as a function of the velocity of the probe particle. Long-dashed and dashed-dotted lines represent the RPA $[-dE/dx]^1$ and $[-dE/dx]^2$ contributions to the Z_1^3 stopping power, respectively. Short-dashed and dotted lines represent contributions to $[-dE/dx]^1$ from the excitation of plasmons and e-h pairs, respectively.

tile potentials. The equipartition rule, valid within first-order perturbation (linear-response) theory cannot be extended to higher orders in the external perturbation.

In order to account approximately for the Z_1^3 effect coming from both the conduction band and the inner shells, a local-plasma approximation was used in Ref. [16], by assuming that a local Fermi energy can be attributed to each element of the solid. The experimental differences between the stopping power of silicon for high-velocity protons and antiprotons [12] were successfully explained in this way. Proton and antiproton stopping powers of a variety of solid targets have been reported recently for projectile velocities near and below the stopping maximum [13]. A comparison of our theory with these experiments requires the inclusion of charge-exchange processes, xc effects, and higher-order nonlinear terms. Work in this direction is now in progress [63].

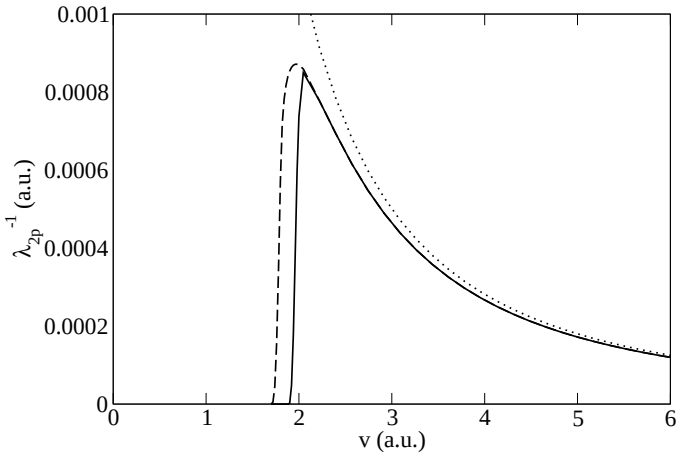

Figure 6: RPA double-plasmon inverse mean free paths of electrons (solid line) and positrons (dashed line) for $r_s = 2.07$, versus the velocity of the projectile, as obtained from Eqs. (27) and (28) by either including (electrons) or excluding (positrons) the step function $\Theta(\omega_{\mathbf{v}-\mathbf{q}} - \varepsilon_F)$. The dotted line is the high-velocity limit dictated by Eq. (50).

3.1.2 Double-plasmon excitation

Single-plasmon contributions to the electron inelastic mean free path of swift electrons have been calculated for many years, both in the high-velocity limit [64] and in the full RPA [65]. Calculations of the double-plasmon contribution to the electron inverse mean free path have been reported in Refs. [19, 20, 21]. Fig. 6 shows our full RPA calculation of the double-plasmon inverse mean free path of swift electrons (solid line) interacting with a FEG, as obtained after introducing Eq. (28) into Eq. (27). Also shown in this figure is the double-plasmon inverse mean free path of swift positrons (dashed line), as obtained by simply removing the step function of Eq. (28), and the high-velocity limit dictated by Eq. (29) multiplied by a factor of 2.16 (dotted line), i.e.,

$$\lambda_{2p}^{-1} \approx 3.13 \times 10^{-3} \frac{\sqrt{r_s}}{v^2}. \tag{50}$$

At high velocities of the projectile the zero-point motion of the target can be neglected. Hence, at these velocities the effect of the Pauli restriction, which only applies to electron probes, is negligible, and the behaviour of

the double-plasmon inverse mean free path is independent of the particle statistics. On the other hand, it is interesting to notice that the high-velocity formula of Eq. (50) gives an excellent account of the full RPA result for both probe electrons and positrons in a wide range of projectile velocities. In particular, for Al and a probe-electron energy of 40 keV Eq. (50) yields a ratio for the double relative to the single plasmon inverse mean free path of 1.9×10^{-3}, in agreement with experiment [18].

3.2 Bounded electron gas

First, we consider a jellium slab of thickness a normal to the z axis, consisting of a fixed uniform positive background of density

$$n_+(z) = \begin{cases} \bar{n}, & -a \leq z \leq 0 \\ \\ 0, & \text{elsewhere,} \end{cases} \tag{51}$$

plus a neutralizing cloud of interacting electrons of density $n(z)$. The positive-background charge density $\bar{n}$ is expressed in terms of the Wigner radius r_s $[1/\bar{n} = (4\pi/3)(r_s\, a_0)^3]$, which we take to be $r_s = 2.07$.

To compute the interacting RPA density-response function of Eq. (32), we follow the method described in Ref. [66]. We first assume that $n(z)$ vanishes at a distance z_0 from either jellium edge [67], and expand the wave functions $\phi_i(z)$ in a Fourier sine series. We then introduce a double-cosine Fourier representation for the density-response function, and find explicit expressions for the stopping power of Eq. (36) in terms of the Fourier coefficients of the density-response function [57]. We take the wave functions $\phi_i(z)$ to be the eigenfunctions of a one-dimensional LDA hamiltonian with use of the Perdew-Zunger parametrization [68] of the Quantum Monte Carlo xc energy of a uniform FEG [69]

Finally, the stopping power of a semi-infinite FEG is obtained with the use of the following relation:

$$-\frac{dE}{dx} = \frac{[-dE/dx]\,(a_n^-) + [-dE/dx]\,(a_n) + [-dE/dx]\,(a_n^+)}{3}, \tag{52}$$

where a_n is the threshold width for which the nth subband for the z motion is first occupied, $a_n^- = a_n - \lambda_F/4$, and $a_n^+ = a_n + \lambda_F/4$, $\lambda_F = 2\pi/(3\pi^2\bar{n})^{1/3}$ being the Fermi wavelength [70]. Converged results have been found with the use of slabs with $n = 12$, for which $a \approx 5 - 6\lambda_F$.

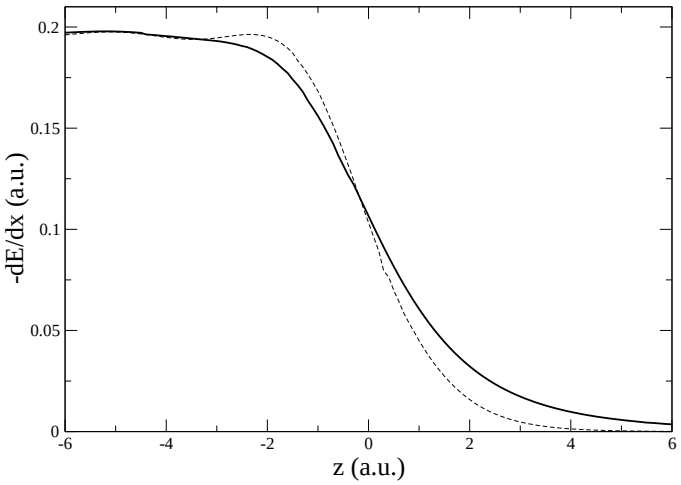

Figure 7: The solid line represents the RPA stopping power of Eq. (36) for $Z_1 = 1$, $r_s = 2.07$, and $v = 2\,v_0$, as a function of the distance z between the surface and the projectile. The solid is in the region $z < 0$. The dashed line represents the LDA stopping power, as obtained by assuming that the actual stopping power of Eq. (36) can be approximated by that of a uniform FEG with the local density $n(z)$.

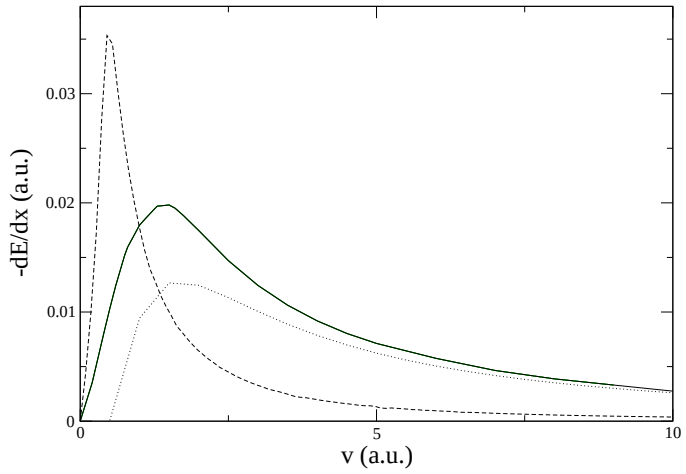

Figure 8: The solid line represents the RPA stopping power of Eq. (36) for $Z_1 = 1$, $r_s = 2.07$, and $z = 3\,a_0 \approx \lambda_F/2$, as a function of the projectile velocity. The dashed line represents the LDA stopping power, as obtained by assuming that the actual stopping power of Eq. (36) can be approximated by that of a uniform FEG with the local density $n(z)$. The dotted line is the high-velocity limit dictated by Eq. (38).

Fig. 7 depicts our full RPA calculation of the stopping power of a semi-infinite FEG, as obtained from Eq. (36) for protons ($Z_1 = 1$) moving with speed $v = 2\,v_0$ parallel to the surface. In the interior of the solid, where the electron density is taken to be constant, the stopping power coincides with the Z_1^2 (linear) RPA stopping power of a uniform FEG (see Fig. 1). Outside the solid, the stopping power decreases with the distance z between the surface and the probe-particle trajectory. Also plotted in Fig. 7 is the result of assuming that the stopping power for a charged particle that moves at a distance z from the surface can be approximated by that of a uniform electron gas with the local density $n(z)$ [71]. Fig. 7 clearly shows that this often-used local-density approximation yields an inaccurate description of the position-dependent stopping power, due to the intrinsic nature of surface-induced single and collective excitations not present within this approach.

As the velocity increases, the energy-loss spectrum of charged particles moving far from the surface into the vacuum is dominated by long-wavelength excitations. In this limit, Eq. (36) yields the classical stopping power dictated

by Eq. (38). This is illustrated in Fig. 8, where the velocity-dependent RPA stopping power of Eq. (36) is represented together with the classical result [see Eq. (38)] for a proton ($Z_1 = 1$) moving in the vacuum at a constant distance $z = 3\,a_0 \approx \lambda_F/2$ from the surface. At low velocities, the energy-loss spectrum is dominated by intermediate and short wavelength excitations, even far from the surface into the vacuum, and a combination of the actual electronic selvage at the surface with the intrinsic nature of surface-induced excitations increases the energy loss with respect to that predicted by Eq. (38). At high velocities, the energy-loss spectrum is dominated by surface-plasmon excitations and the full RPA stopping power nicely converges with the classical result. As in Fig. 7, the local-density approximation is also represented in this figure, showing that this often-used approximation cannot account for the energy loss originated in surface-induced excitations, not even at low velocities where the energy loss is entirely due to the excitation of e-h pairs.

3.3 Periodic crystals

In the case of periodic crystals, we first expand the one-electron $\phi_{\mathbf{k},n}(\mathbf{r})$ eigenfunctions in a plane-wave basis,

$$\phi_{\mathbf{k},n}(\mathbf{r}) = \frac{1}{\sqrt{\Omega}} \sum_{\mathbf{G}} u_{\mathbf{k},n}(\mathbf{G}) \mathrm{e}^{\mathrm{i}(\mathbf{k}+\mathbf{G})\cdot\mathbf{r}}, \tag{53}$$

with a kinetic-energy cutoff that varies from 12 Ry in the case of Al ($\sim 100\,\mathbf{G}$-vectors) to 16 Ry in the case of Si ($\sim 300\,\mathbf{G}$-vectors). The coefficients $u_{\mathbf{k},n}$ are evaluated by solving the Kohn-Sham equation of DFT in the LDA with use of the Perdew-Zunger parametrization [68] of the Quantum Monte Carlo xc energy of a uniform FEG [69]. The electron-ion interaction is based on the use of an *ab initio* non-local, norm-conserving ionic pseudopotential [72]. Then, Eq. (43) is used to evaluate the Fourier coefficients of the noninteracting density-response function, and a matrix equation [Eq. (41)] is solved for the Fourier coefficients of the interacting RPA density-response function.

Here we present new calculations for the random stopping power of Al and Si, which represent an extension of existing first-principles calculations [38, 40] by allowing transitions with larger values of the momentum transfer.

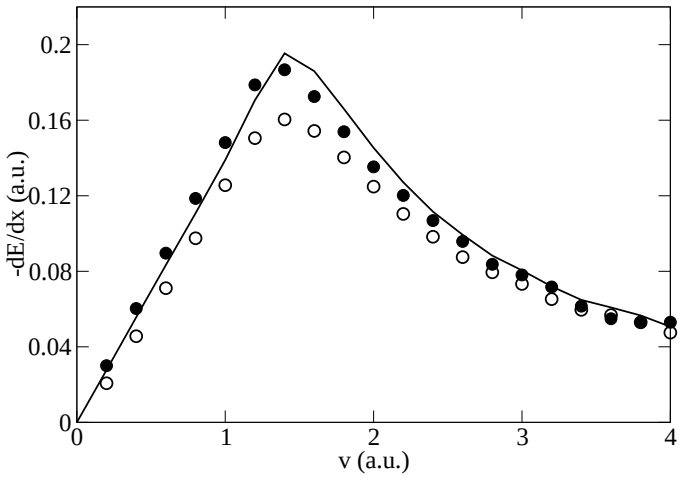

Figure 9: First-principles RPA calculation of the random stopping power of valence electrons in Al (solid circles) and Si (open circles) for protons and antiprotons ($Z_1^2 = 1$), versus the projectile velocity, as obtained from Eq. (46). These results have been found to be rather insensitive to the choice of the direction of the projectile velocity. The solid line represents the Z_1^2 (linear) stopping power of a uniform FEG with $r_s = 2$.

3.3.1 Random stopping power

Fig. 9 shows our first-principles first-order (linear-response) RPA calculation of the random stopping power of valence electrons in Al (solid circles) and Si (open circles) for protons and antiprotons ($Z_1^2 = 1$), as obtained from Eq. (46) [73]. Since the electron density of valence electrons in Al ($r_s = 2.07$) and Si ($r_s = 2.01$) is nearly the same, within a FEG model of the solid the stopping powers of Al and Si are expected to coincide (solid line of Fig. 9). Nevertheless, our first-principles calculations indicate that this is not the case. At low projectile velocities (where only valence electrons contribute to the energy loss of the projectile), the stopping power of Si is considerably smaller than that of Al, in agreement with available measurements of the stopping power of this materials for either protons [74, 75] and antiprotons [13]. While the stopping power of Al is found to be slightly larger than in the case of a FEG, the band gap of Si yields a stopping power of this material that is smaller than in the case of a FEG.

At high velocities, well above the stopping maximum, the sum over the

frequency ω in Eq. (46) can be replaced by an integration over all positive frequencies, and the sum rule

$$\int_0^\infty \mathrm{d}\,\omega\,\omega \mathrm{Im} K^{-1}_{\mathbf{G},\mathbf{G}'}(\mathbf{q},\omega) = 2\pi^2\, n_{\mathbf{G}-\mathbf{G}'} \tag{54}$$

($n_{\mathbf{G}}$ represents the Fourier components of the density, $n_{\mathbf{G}=0}$ being the average electron density n of the crystal) yields a stopping power which depends on n but not on the details of the band-structure of the target material:

$$\left[-\frac{\mathrm{d}E}{\mathrm{d}x}\right]_{\mathrm{random}} \sim \frac{4\pi Z_1^2}{v^2}\, n\, \ln\frac{2v^2}{\omega_p}. \tag{55}$$

Hence, at high velocities the stopping powers of valence electrons in Al and Si both coincide with that of a FEG with the same electron density (see Fig. 9).

While at low velocities the contribution to the total energy loss due to excitation of inner-shell electrons is negligible, at velocities larger than the Fermi velocity it is necessary to allow for this contribution. The cross sections for the ionization of inner shells in Al were obtained by Ashley *et al.* [76] in the first-Born approximation utilizing atomic generalized oscillator strength functions. By adding the contribution from core electrons to that of valence electrons (this contribution was calculated within a FEG model of the solid) these authors found a nice agreement with experiment. Good agreement with experiment was also shown in Ref. [2] by adding to the valence-electron energy loss of a FEG with $r_s = 2.01$ the energy loss from core electrons in Si as taken from Walske's calculations [77].

4 Summary and conclusions

We have presented a survey of current investigations of various aspects of the interaction of charged particles with solids.

In the framework of many-body perturbation theory, we have studied the nonlinear interaction of charged particles with a free gas of interacting electrons. We have presented general procedures to calculate the nonlinear potential induced by charged particles moving in an inhomogeneous electron system, the Z_1^3 contribution to the stopping power of a FEG, and double-plasmon excitation probabilities.

Our calculations for the RPA stopping power of a FEG indicate that for velocities smaller than the Fermi velocity the stopping power is, up to third order in the projectile charge, a linear function of the velocity of the projectile. Our calculations also indicate that the high-velocity limit dictated by Eq. (20) gives an excellent account of the full RPA result in a wide range of projectile velocities. By assuming that a local Fermi energy can be attributed to each element of the solid target, the experimental differences between the stopping power of silicon for high-velocity protons and antiprotons [12] were succesfully explained in Ref. [16].

New calculations of the various contributions to the second-order stopping power of a uniform FEG coming from the excitation of e-h pairs and plasmons have been reported. We have found that the equipartition rule, valid within first-order perturbation (linear-response) theory, cannot be extended to higher orders in the external perturbation. We have also found that contributions from collective excitations to the Z_1^3 term are small.

New RPA double-plasmon inverse mean free paths of electrons and positrons have been evaluated, with explicit introduction of recoil and probe-particle statistics. The high-velocity limit of Eq. (50) is found to give an excellent account of the full RPA double-plasmon inverse mean free paths in a wide range of projectile velocities. This formula [Eq. (50)] yields for Al and a probe-electron energy of 40 keV a ratio for the double relative to the single plasmon inverse mean free path of 1.9×10^{-3}, in agreement with experiment [18].

We have reviewed existing self-consistent calculations of the energy loss of charged recoiless particles moving parallel to a plane-bounded FEG, in the framework of linear response theory. In the high-velocity limit and for charged particles moving far from the surface into the vacuum the actual stopping power is found to converge with the classical limit dictated by Eq. (38). However, at low and intermediate velocities substantial changes in the stopping power are observed as a realistic description of the surface response is considered, which leads to the conclusion that a self-consistent description of the surface response is necessary if one is to look at the energy loss of charged particles moving outside a solid surface. Accurate measurements of the energy loss of protons being reflected from a variety of solid surfaces at grazing incidence have been reported [78, 79, 80]. A theoretical description of these experiments requires that the ion trajectory $z(t)$ be calculated and energy losses from the excitation of inner shells be taken into account. Work in this direction is now in progress.

Finally, we have extended existing first-principles calculations of the random stopping power of valence electrons in Al and Si by allowing transitions to larger values of the momentum transfer. We have found that at low velocities (where losses from the excitation of inner shells is negligible) the random stopping power of Si is considerably smaller than that of Al, though both Al and Si have nearly the same valence-electron density. At high velocities, band-structure effects become negligible and the random stopping power of valence electrons in Al and Si nearly coincide.

A quantitative comparison of our theory with existing measurements of the energy loss of antiprotons [13] (which unlike protons carry no bound states) in a variety of target materials can be achieved by combining our first-principles calculations of the Z_1^2 (linear-response) stopping power with Z_1^3 corrections in a FEG. Nevertheless, a comparison with experiment still requires the inclusion of losses from the inner shells, xc effects, and higher-order nonlinear terms. Work in this direction is now in progress.

Acknowledgements

We acknowledge partial support by the University of the Basque Country, the Basque Unibertsitate eta Ikerketa Saila, and the Spanish Ministerio de Ciencia y Tecnología.

References

[1] P. M. Echenique, F. Flores, Solid State Phys. **43**, 229 (1990).

[2] M. A. Kumakhov and F. F. Komarov, *Energy Loss and Ion Ranges in Solids* (Gordon and Breach, New York, 1981).

[3] Philos Mag. **25**, 10 (1913); **30**, 581 (1915).

[4] H. A. Bethe, Ann. Phys. (Leipzig) **5**, 325 (1930).

[5] D. Bohm and D. Pines, Phys. Rev. **82**, 625 (1951); D. Pines and D. Bohm, Phys. Rev. **85**, 338 (1952); D. Bohm and D. Pines, Phys. Rev. **92**, 609 (1953); D. Pines, Phys. Rev. **92**, 626 (1953).

[6] J. Lindhard, K. Dan. Vidensk. Selsk. Mat.-Fys. Medd. **28**, no.8 (1954).

[7] J. Hubbard, Proc. Phys. Soc. (London) **243**, 336 (1957).

[8] K. S. Singwi, M. P. Tosi, R. H. Land, and A. Sjolander, Phys. Rev. **176**, 589 (1968); K. S. Singwi, A. Sjolander, M. P. Tosi, and R. H. Land, Phys. Rev. B **1**, 1044 (1970); K. S. Singwi and M. P. Tosi, Solid State Phys. **36**, 177 (1981).

[9] S. L. Adler, Phys. Rev. **126**, 413 (1962); N. Wiser, Pys. Rev. **129**, 62 (1963).

[10] N. D. Mermin, Phys. Rev. B **1**, 2362 (1970).

[11] W. H. Barkas, W. Birnbaum, and F.M . Smith, Phys. Rev. **101**, 778 (1956); W. H. Barkas, N. J. Dyer, and H. H. Heckman, Phys. Rev. Lett. **11** 26 (1963); **11** 138(E) (1963).

[12] L. H. Andersen, P. Hvelplund, H. Knudsen, S.P. Moller, J. O. P. Pedersen, E. Uggerhoj, K. Elsener, and E. Morenzoni, Phys. Rev. Lett. **62**, 1731 (1989).

[13] S. P. Moller, E. Uggerhoj, H. Bluhme, H. Knudsen, U. Mikkelsen, K. Paludan, and E. Morenzoni, Phys. Rev. A **56** 2930 (1997); S. P. Moller, A. Csete, T. Ichioka, H. Knudsen, U. I. Uggerhoj, and H. H. Andersen, Phys. Rev. Lett **88**, 193201 (2002).

[14] J. C. Ashley, R. H. Ritchie, and W. Brandt, Phys. Rev. B **5,** 2393 (1972); **8**, 2402 (1973); **10**, 737 (1974).

[15] C. C. Sung and R. H. Ritchie, Phys. Rev. A **28**, 674 (1983); C. D. Hu and E. Zaremba, Phys. Rev. B **37**, 9268 (1988); H. Mikkelsen and P. Sigmund, Phys Rev. A **40**, 101 (1989); H. Esbensen and P. Sigmund, Ann. Phys. **201**, 152 (1990).

[16] J. M. Pitarke, R. H. Ritchie, and P. M. Echenique, Nucl. Instrum. Methods B **79**, 209 (1993); J. M. Pitarke, R. H. Ritchie, P. M. Echenique, and E. Zaremba, Europhys. Lett. **24**, 613 (1993).

[17] J.C. Spence and A.E. Spargo, Phys. Rev. Lett. **26** 895 (1971).

[18] P. Schattschneider, F. Fodermayr and D.S Su, Phys. Rev. Lett. **59**, 724 (1987).

[19] J. C. Ashley and R. H. Ritchie, Phys. Stat. Sol. **38**, 425 (1970).

[20] J. M. Pitarke and R. H. Ritchie, Nucl. Instrum. Methods B **90**, 358 (1994).

[21] I. Campillo and J. M. Pitarke, Nucl Instrum. Methods B **115**, 75 (1996). Eq. (10) here replaces Eq. (23) of Ref. [20].

[22] A. Arnau and E. Zaremba, Nucl. Instrum. Methods B **90**, 32 (1994); J. J. Dorado, O. H. Crawford, and F. Flores, Nucl. Instrum. Methods B **93**, 175 (1994); erratum, Nucl. Instrum. Methods B **95**, 144 (1995).

[23] J. M. Pitarke, A. Bergara, and R. H. Ritchie, Nucl. Instrum. Methods B **99**, 87 (1995); A. Bergara and J. M. Pitarke, Nucl. Instrum. Methods B **96**, 604 (1995); A. Bergara, I. Campillo, J. M. Pitarke, and P. M. Echenique, Phys. Rev. B **56**, 15654 (1997).

[24] M. J. Puska and R. M. Nieminen, Phys. Rev. B **27**, 6121 (1983).

[25] P. M. Echenique, R. M. Nieminen, and R. H. Ritchie, Solid State Commun. **37** 779 (1981); P. M. Echenique, R. M. Nieminen, J. C. Ashley, and R. H. Ritchie, Phys. Rev. A **33**, 897 (1986); J. C. Ashley, R. H. Ritchie, P. M. Echenique, and R. M. Nieminen, Nucl. Instrum. Methods B **15**, 11 (1986).

[26] P. Hohenberg and W. Kohn, Phys. Rev. **136**, B864 (1964); W. Kohn and L. J. Sham **140**, A1133 (1965).

[27] E. Zaremba, A. Arnau, and P. M. Echenique, Nucl. Instrum. Methods B **96**, (1995).

[28] W. Brandt and M. Kitagawa, Phys. Rev. B **25**, 5631 (1982).

[29] J. M. Pitarke, R. H. Ritchie, and P. M. Echenique, Phys. Rev. B **52**, 13883 (1995).

[30] F. F. Komarov and M. A. Kumakhov, Rad. Effects **22**, 1 (1974).

[31] A. Desalvo and R. Rosa, J. Phys. C **10**, 1595 (1977).

[32] H. Esbensen and J. A. Golovchenko, Nucl. Phys. A **298**, 382 (1978).

[33] A. F. Burenkov, F. F. Komarov, and M. A. Kumakhov, Phys. Status Solidi B **99**, 417 (1980).

[34] O. H. Crawford and C. W. Nestor, Phys. Rev. A **28**, 1260 (1983).

[35] P. L. Grande and G. Schiwietz, Phys. Lett. A **163**, 439 (1992).

[36] J. J. Dorado and F. Flores, Phys. Rev. A **47**, 3062 (1993).

[37] T. M. H. E. Tielens, Gerrit E. W. Bauer and T. H. Stoof, Phys. Rev. B **49**, 5741 (1994).

[38] I. Campillo, J. M. Pitarke, A. G. Eguiluz and A. García, Nucl. Instrum. and Methods B **135**, 103 (1998); I. Campillo, J. M. Pitarke, and A. G. Eguiluz, Phys. Rev. B **58**, 10307 (1998).

[39] R. J. Mathar, J. R. Sabin, and S. B. Trickey, Nucl. Instrum. Methods B **155**, 249 (1999).

[40] J. M. Pitarke and I. Campillo, Nucl. Instrum. Methods B **164**, 147 (2000); I. Campillo and J. M. Pitarke, Nucl. Instrum. Methods B **164**, 161 (2000).

[41] This approximation is valid for heavy charged particles, e.g., ions, and also for swift electrons moving with velocities that are large compared to those of the electrons in the medium. In the case of electrons, $Z_1 = -1$.

[42] F. Flores and F. García Moliner, *Introduction to the Theory of Solid Surfaces* (Cambridge University Press, Cambridge, 1979).

[43] T. del Río and J. M. Pitarke, Phys. Rev. B **62**, 6862 (2000).

[44] T. del Río and J. M. Pitarke, J. Phys. A **34**, 7607 (2001).

[45] V. U. Nazarov and S. Nishigaki, Phys. Rev. B **65**, 94303 (2002).

[46] M. Petersilka, U. J. Gossmann, and E. K. U. Gross, Phys. Rev. Lett. **76**, 1212 (1996).

[47] A. L. Fetter and J. D. Wallecka, *Quantum theory of Many Particle Systems* (MacGraw-Hill, New York, 1964).

[48] R. M. Dreizler and E. K. U. Gross, *Density Functional Theory* (Springer-Verlag, Berlin, 1990).

[49] F. Aryasetiawan and O. Gunnarsson, Rep. Prog. Phys. **61**, 237 (1998).

[50] M. Nekovee and J. M. Pitarke, Comput. Phys. Commun. **137**, 123 (2001).

[51] In usual practice, all single-particle wave functions and energies are typically obtained by solving the single-particle Kohn-Sham equation of density-functional theory in the so-called local-density approximation (LDA) [see, e.g., Ref. [48]].

[52] R. Cenni and P. Saracco, Nuclear Phys. A **487**, 279 (1988).

[53] C. F. Richardson and N. W. Ashcroft, Phys. Rev. B **50**, 8170 (1994).

[54] G. D. Azevedo, P. L. Grande, M. Behar, J. F. Dias, and G. Schiwietz, Phys. Rev. Lett. **86**, 1482 (2001).

[55] The lowest-order double-plasmon Z_1^3 contributions to the inverse mean free path are of third order in the RPA screened interaction $v_{\mathbf{q}}K_{\mathbf{q},\omega}$. Although these contributions to the double-plasmon inverse mean free path are of lower order in $v_{\mathbf{q}}K_{\mathbf{q},\omega}$ than the Z_1^2 contribution of Eq. (28), which is of fourth order in the RPA screened interaction, they decrease as v^{-5} and are therefore found to be negligible for the velocities of interest.

[56] A. Bergara, J. M. Pitarke, and R. H. Ritchie, Phys. Rev. B **60**, 16176 (1999).

[57] A. García-Lekue and J. M. Pitarke, Phys. Rev. B **64**, 35423 (2001); Phys. Rev. B **67**, 89902(E) (2003); Nucl. Instrum. Methods B **182**, 56 (2001); J. Electron Spectrosc. **129**, 223 (2003).

[58] D. S. Gemmell, Rev. Mod. Phys. **46**, 129 (1974).

[59] R. H. Ritchie, Phys. Rev. **106**, 874 (1957).

[60] A. Liebsch, Phys. Rev. Lett. **71**, 145 (1993); A. Liebsch, *Electronic Excitations at Metal Surfaces* (Plenum, New York, 1997).

[61] P. M. Echenique and J. B. Pendry, J. Phys. C **8**, 2936 (1975).

[62] J. Lindhard and A. Winther, K. Dan. Vidensk. Selsk. Mat.-Fys. Medd. **34**, no.4 (1964).

[63] V. U. Nazarov and J. M. Pitarke (unpublished).

[64] D. Pines, Phys. Rev. **85**, 931 (1952).

[65] C. J. Tung and R. H. Ritchie, Phys. Rev. B **16**, 4302 (1977).

[66] A. G. Eguiluz, Phys. Rev. Lett. **51**, 1907 (1983); Phys. Rev. B **31**, 3303 (1985).

[67] z_0 is chosen sufficiently large for the physical results to be insensitive to the precise value employed.

[68] J. Perdew and A. Zunger, Phys. Rev. B **23**, 5048 (1981).

[69] D. M. Ceperley and B. J. Alder, Phys. Rev. Lett. **45**, 566 (1980).

[70] J. M. Pitarke and A. G. Eguiluz, Phys. Rev. B **57**, 6329 (1998); Phys. Rev. B **63**, 45116 (2001).

[71] The use of this local-density approximation, in which one replaces $-(dE/dx)(z)$ of Eq. (36) by the stopping power of a uniform electron gas of density $n(z)$, should not be confused with the use of an LDA xc potential in DFT.

[72] D. R. Hamann, M. Schluter, and C. Chiang, Phys. Rev. Lett. **43**, 1494 (1979); D. R. Hamann, Phys. Rev. B **40**, 2980 (1989).

[73] Random stopping powers of valence electrons in Al and Si have been calculated with the integrations over the momentum transfer being extended from zero to $2.9\,q_F$ and $2.6\,q_F$ for Al and Si, respectively.

[74] J. F. Ziegler, J. P. Biersack, and U. Littmark, *The stopping and range of ions in solids*, Vol. 1 (Pergamon, New York, 1985).

[75] P. Bauer, Nucl. Instrum. Methods B **45**, 673 (1990).

[76] J. C. Ashley, C. J. Tung, and R. H. Ritchie, Surf. Sci. **81**, 409 (1979); C. J. Tung, J. C. Ashley, and R. H. Ritchie, Surf. Sci. **81**, 427 (1979).

[77] M. C. Walske, Phys. Rev. **101**, 940 (1956).

[78] K. Kimura, M. Hasegawa, and M. Mannami, Phys. Rev. B **36**, 7 (1987).

[79] Y. Fuji, S. Fujiwara, K. Narumi, K. Kimura, and M. Mannami, Surf. Sci. **277**, 164 (1992); K. Kimura, H. Kuroda, M. Fritz, and M. Mannami, Nucl. Instrum. Methods B **100**, 356 (1995).

[80] H. Winter, M. Wilke, and M. Bergomaz, Nucl. Instrum. Methods B **125**, 124 (1997).